DEVELOPMENTAL DYNAMICS 247:509–520, 2018
DOI: 10.1002/DVDY.24521

RESEARCH ARTICLE

Endocardial Fibroelastosis is Secondary to Hemodynamic Alterations in the Chick Embryonic Model of Hypoplastic Left Heart Syndrome

Zivorad Pesevski,[1,2] Alena Kvasilova,[1] Tereza Stopkova,[1] Ondrej Nanka,[1] Eliska Drobna Krejci,[1,2] Christine Buffinton,[3] Radka Kockova,[2,4] Adam Eckhardt,[2] and David Sedmera [1,2]*

[1]Institute of Anatomy, Charles University, Prague, Czech Republic
[2]Institute of Physiology, Academy of Sciences of the Czech Republic, Prague, Czech Republic
[3]Department of Mechanical Engineering, Bucknell University, Lewisburg, Pennsylvania
[4]Institute of Clinical and Experimental Medicine, Prague, Czech Republic

Background: Endocardial fibroelastosis (EFE) is a diffuse thickening of the ventricular endocardium, causing myocardial dysfunction and presenting as unexplained heart failure in infants and children. One of the postulated causes is persistent and increased wall tension in the ventricles. **Results:** To examine whether reduced ventricular pressure in a chick model of hypoplastic left heart syndrome (HLHS) induced by left atrial ligation (LAL) at embryonic day (ED) 4 is associated with EFE at later stages, myocardial fibrosis was evaluated by histology and immunoconfocal microscopy and mass spectrometry (MS) at ED12. Immunohistochemistry with collagen I antibody clearly showed a significant thickening of the layer of subendocardial fibrous tissue in LAL hearts, and MS proved this significant increase of collagen I. To provide further insight into pathogenesis of this increased fibroproduction, hypoxyprobe staining revealed an increased extent of hypoxic regions, normally limited to the interventricular septum, in the ventricular myocardium of LAL hearts at ED8. **Conclusions:** Abnormal hemodynamic loading during heart development leads to myocardial hypoxia, stimulating collagen production in the subendocardium. Therefore, EFE in this chick embryonic model of HLHS appears to be a secondary effect of abnormal hemodynamics. *Developmental Dynamics 247:509–520, 2018.* © 2017 Wiley Periodicals, Inc.

Key words: Hypoxia; HLHS; left atrial ligation; collagen; chick embryo

Submitted 17 January 2017; First Decision 1 May 2017; Accepted 10 May 2017; Published online 20 May 2017

Introduction

The term endocardial fibroelastosis (EFE), a thickening of the subendocardial layer of ventricles due to an increased deposition of connective and elastic fibers, was first introduced by Weinberg and Himmelfarb in 1943 (Weinberg and Himmelfarb, 1943). The EFE can be primary or secondary. Primary EFE is not associated with other significant morphological or structural abnormalities of the heart. Secondary EFE is associated with various congenital heart diseases (Angelov et al., 1984), most notably hypoplastic left heart syndrome (HLHS) (Essed et al., 1975) and aortic stenosis or atresia (Achiron et al., 1988), but also maternal autoimmune diseases (Nield et al., 2002). Other developmental abnormalities in HLHS include underdevelopment of the left atrium and ventricle, deformed or very small mitral and aortic valves, and the right ventricle rather the left forming the apex of the heart (Bohlmeyer et al., 2003; Sedmera et al., 2005). In the United States alone, approximately 2000 infants with HLHS are born annually (Bradley, 1999). Despite its low incidence relative to other congenital cardiac disorders, HLHS, if left untreated, is responsible for 25–40 percent of all neonatal cardiac deaths. The exact cause of HLHS is still unknown. Some studies have suggested diverse genetic, cellular, and molecular mechanisms of HLHS (Grossfeld, 1999; Sedmera et al., 2002; Bohlmeyer et al., 2003; Loffredo et al., 2004). Despite many theories about its cause, the origin is clearly multifactorial, complicating detailed mechanistic analysis. Frequent association of EFE with HLHS led us to hypothesize that abnormal hemodynamic loading is an important factor in its pathogenesis.

Despite recent isolation of mutant mouse lines with HLHS, the previously established models in fetal lamb (Fishman et al., 1978) or embryonic chick (Harh et al., 1973; Rychter and Rychterova, 1981; Sedmera et al., 1999) are based on hemodynamic alterations. Experimentally decreased blood flow to the left heart structures

Grant sponsor: Ministry of Education; Youth and Sports of the Czech Republic PROGRESS-Q38; Charles University UNCE 204013; SVV Graduate Student Training Program; Czech Academy of Sciences RVO: 67985823; Ministry of Health 17-28265A; Grant Agency of the Czech Republic, P302/11/1308 and 16-02972S.
*Correspondence to: David Sedmera, Charles University in Prague, First Faculty of Medicine, Institute of Anatomy, U Nemocnice 3, 12800 Prague 2, Czech Republic. E-mail: david.sedmera@lf1.cuni.cz

Article is online at: http://onlinelibrary.wiley.com/doi/10.1002/dvdy.24521/abstract

leads to hypoplasia of the left atrium, ventricle, and the aorta, with compensatory abnormal development of the right-sided structures. However, detailed influence of the abnormal hemodynamics on the myocardial structure, apart from showing deficiency in proliferation and growth factor expression (Sedmera et al., 2002) were so far not investigated, especially not during the later phases of cardiac development. These later phases are, however, important for eventual utility of the hypoplastic left ventricle for biventricular circulation, as during the early phases the changes are reversible (deAlmeida et al., 2007).

It has been reported that human EFE has a strong relationship with decreased left ventricular blood flow, which has been mimicked by heterotopic heart transplantation in mouse and rat EFE models. In the rat model, Friehs and coworkers (Friehs et al., 2013) showed that neonatal (corresponding developmentally to human fetal) but not 2-week-old hearts transplanted into adult rats develop EFE consisting of collagen and elastin deposition with scarce cellular and vascular components, pointing to a critical time window for development of hemodynamically induced EFE. In a mouse model, endocardial-to-mesenchymal transformation was demonstrated as a source of this increase in subendocardial tissue (Xu et al., 2015), and it was shown to be regulated by TGF-β/BMP5 and 7 signaling, pointing to BMP7 as a potential therapeutic target for treatment of EFE and its restriction of heart growth.

Normal embryonic development involves physiological tissue hypoxia. Hypoxic regions in the heart were associated with the areas of developing cardiac conduction system (Wikenheiser et al., 2006). The degree of tissue-level oxygen concentration is responsible for inducing expression of multiple signaling pathways via hypoxia-inducible factors, especially HIF-1α. The goal of these pathways is to optimize metabolic events in different tissues (e.g., stimulation of erythropoiesis, angiogenesis, regulation of glycolysis). The degree of hypoxia also influences myocardial architecture and the status of the coronary vasculature (Nanka et al., 2008).

Hypoxia is also important in the process of healing, where it orchestrates production of extracellular matrix (ECM). Hypoxia-induced periostin expression is regulated by HIF-1α. Periostin in turn activates the αvβ3 integrin-PI3K/Akt pathway. These findings suggest that hypoxia initiates hyperplasia and increases periostin expression under hypoxic conditions; periostin is involved in the pathogenesis of keloids and fibroproliferative disorders (Zhang et al., 2014). Increased periostin expression affects the proliferation, collagen synthesis, migration, and invasion of keloid fibroblasts under hypoxic conditions.

This study tests the theory proposed by Essed and collaborators (Essed et al., 1975) linking abnormal hemodynamics, hypoxia, and increased fibrosis in a chick model of HLHS induced by left atrial ligation (LAL) (Sedmera et al., 1999). We observed well established EFE at later stages that was secondary to the hemodynamic alterations in this condition, possibly underlined by abnormal ventricular strains and myocardial hypoxia.

Results

To induce hemodynamically the phenotype of left heart hypoplasia mimicking the human HLHS, we performed in ED4 chick embryos partial ligation of the left atrial appendage (Sedmera et al., 1999). The survival in the embryos with LAL group was 75% until ED6, 50% until ED8, and 20% until ED12. Approximately one-third of the operated embryos had the desired phenotype (apex-forming right ventricle) at ED6, one-half at ED8, and one-quarter at ED12, suggesting gradual development of the phenotype as well as negative selection against the most severe cases. Survival of the LAL embryos until ED6 in the ex ovo culture was about 50% and only very rarely until ED8 (deAlmeida et al., 2007), limiting the meaningful functional analysis to a single time point.

Phenotypic analysis at ED12, performed only on the hearts with clear phenotype defined as apex-forming right ventricle (Sedmera et al., 2005), showed the presence of Alcian blue-positive extracellular matrix in the area of the cardiac skeleton, valves, and adventitia of the great vessels (Fig. 1), as well as in a thin layer underneath the endocardium. This collagen-positive subendocardial layer was significantly increased in both ventricles of the LAL hearts (Figs. (1 and 2)), and also showed also increased positivity for periostin (Figs. (1 and 3)), especially in the right ventricle. Anti–smooth muscle actin (SMA) staining visualized the developing smooth muscle coat of the coronary vessels, but did not detect any myofibroblasts in the normal or thickened subendocardium of the LAL hearts (Fig. 4). In addition, there were SMA-positive cells present in the mesenchyme of the dysplastic right atrioventricular valve, but not in the mitral valve, in the LAL hearts.

Mass spectrometry (MS) on samples of eight control and eight LAL hearts validated the apparent increase of collagen in the LAL hearts at ED12 (Fig. 5). Collagen I content increased significantly in the whole LAL hearts, more pronounced in the left than in the right ventricle, but statistically significant only in the right.

To assess the possible role of hypoxia in development of EFE, we performed hypoxyprobe staining at ED8, (i.e., prior to appearance of a significant increase in fibrosis). Histological examination of control ED8 hearts did not show a significant increase in deposition of collagen and periostin in the subendocardium at that stage, with only small amounts of fibrous staining present in the developing cardiac skeleton, valves, and outflow vessels. Hypoxyprobe staining, normally limited in the heart only to small islands in the interventricular septum and patches in the left ventricular free wall (Fig. 6), showed a large positivity in both the septum and ventricular compact layer of LAL hearts; however, no increase in periostin, collagen I, or Alcian blue staining was detected at this point.

Echocardiographic analysis at ED6 showed that the left ventricle of the LAL embryos already had a significantly smaller cross-sectional area compared with the control left ventricle and compared with the right ventricle of the same heart (Fig. 7). The contractile function of the smaller left ventricle, expressed by ejection fraction (control: 28.7 ± 8.1 vs. LAL: 29.3 ± 11.2; $P = 0.9$), circumferential strain, and longitudinal strain, appeared relatively normal (Fig. 6); however, the radial strain was significantly lower in the LAL left ventricle. In the right ventricles, the longitudinal strain was significantly higher in the LAL group. The circumferential-to-longitudinal strain ratio was not significantly different between the control left and right ventricles; however, in the LAL hearts, because the longitudinal strain was significantly higher in the right ventricle, the circumferential-to-longitudinal strain ratio was significantly changed in LAL right ventricle, while in the left ventricle the changes vs. controls were nonsignificant. The radial strain did not differ significantly between the left and right ventricles in the control hearts, while

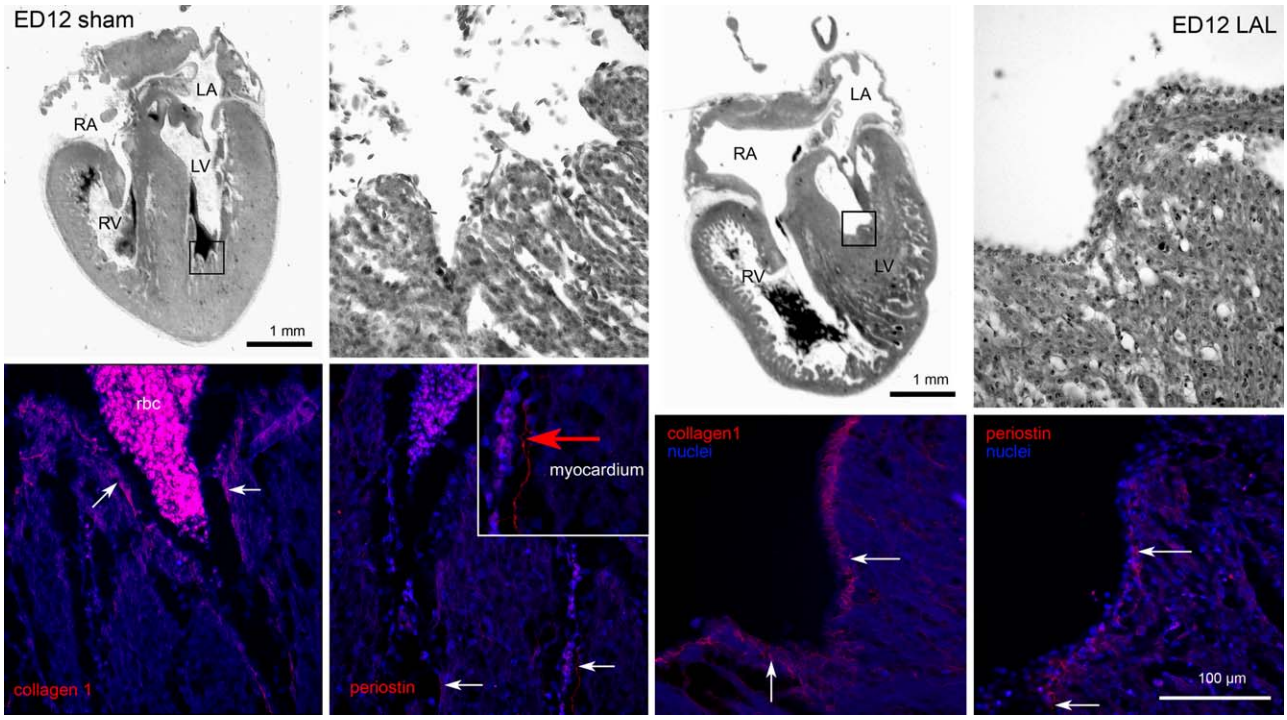

Fig. 1. Histology of ED12 chick embryonic heart. In the control (sham-operated) heart, the left ventricle forms the apex, and Alcian blue staining is limited to the developing cardiac skeleton, valves, and subepicardium. Immunoconfocal microscopy shows positive collagen I staining in the subendocardium (arrows), which is also positive for periostin. In the LAL heart, the apex is formed by the right ventricle. Collagen staining in the subendocardium (arrows) is more prominent, as is the immunostaining for periostin. LA, left atrium; LV, left ventricle; RA, right atrium; RV, right ventricle. Further examples of periostin staining can be found in Figure. 3.

in the LAL group, the left ventricular values were significantly lower than in the right ventricle.

Three-dimensional reconstructions confirmed the significantly smaller left ventricular tissue volume in the LAL group, $0.49 \pm 0.09\,mm^3$ ($n = 7$) vs. $0.89 \pm 0.06\,mm^3$ in the controls ($n = 10$) ($P < 0.0001$) already at this time interval (Fig. 8). Histological staining at this stage did not reveal any differences between control and LAL hearts in any of the parameters of fibrosis (data not shown).

Discussion

Human hearts developing the HLHS phenotype show hypoplasia of the left side of the heart (mitral and aortic valves, left ventricle) (Sedmera et al., 2005). This left-sided hypoplasia is faithfully reproduced using the experimental chick model of left atrial ligation, where hemodynamic changes lead to gradual development of HLHS (Sedmera et al., 1999). The chick model has been successfully used to test the feasibility of prenatal interventions aimed at salvaging the functional left ventricle (deAlmeida et al., 2007; de Almeida and Sedmera, 2009). In this study, we explored the hypothesis that EFE observed in the clinical settings could be due to hemodynamic alterations inherent to this condition.

Our results show that during the development of the phenotype (ED6), the early function of the left ventricle is relatively normal, and indeed the changes were found to be reversible by secondary hemodynamic intervention correcting the abnormal loading at ED8 (deAlmeida et al., 2007). However, at this stage, increased tissue hypoxia was already evident (Fig. 6), which helps to explain previously reported disregulation of angiogenic growth factors (Sedmera et al., 2002), as well as anomalies in coronary vasculature (Dbaly and Rychter, 1967) and later increase in fibrosis at ED12 (Figs. 3,5). It is interesting to point out that the hypoxic regions prevailed in the thickest areas of the myocardium, while the later deposition of the collagen was found strictly in the subendocardium; this could be explained by signaling of the hypoxic myocardium stimulating endocardial-to-mesenchymal transformation leading to fibrosis, postulated to be the source of the EFE tissue (Xu et al., 2015).

We have studied tissue-level hypoxia at several time points (ED6, ED8, ED12) and found that at ED6, there was no difference compared to control (very few hypoxic areas), while at ED8 and ED12, the changes were quite distinct. However, the changes in extracellular matrix are trickier to measure. At ED6, there is very little collagen detectable either on section (histological staining of antibody) or by MS. The amounts were likewise very low, and no difference could be found between LAL and control hearts. Only at ED12 did we find a significant increase. Microdissection of fresh hearts was used only for separating the left and right ventricles. It is necessary to carefully trim the hearts, as the valves and great arteries contain high amounts of collagen, and their inclusion would contaminate the sample and obscure any potential differences in the ventricular myocardium.

This time course (altered hemodynamics => hypoxia => fibrosis), while rather logical, is correlative and does not prove causality, which is the main limitation of the present study. Other explanations for the source and cause for fibrosis should be considered: First, it is possible that the observed hypoxia is secondary to the changes in endocardial basement membrane architecture, limiting oxygen delivery to the subendocardium from the ventricular lumen. We do not consider this

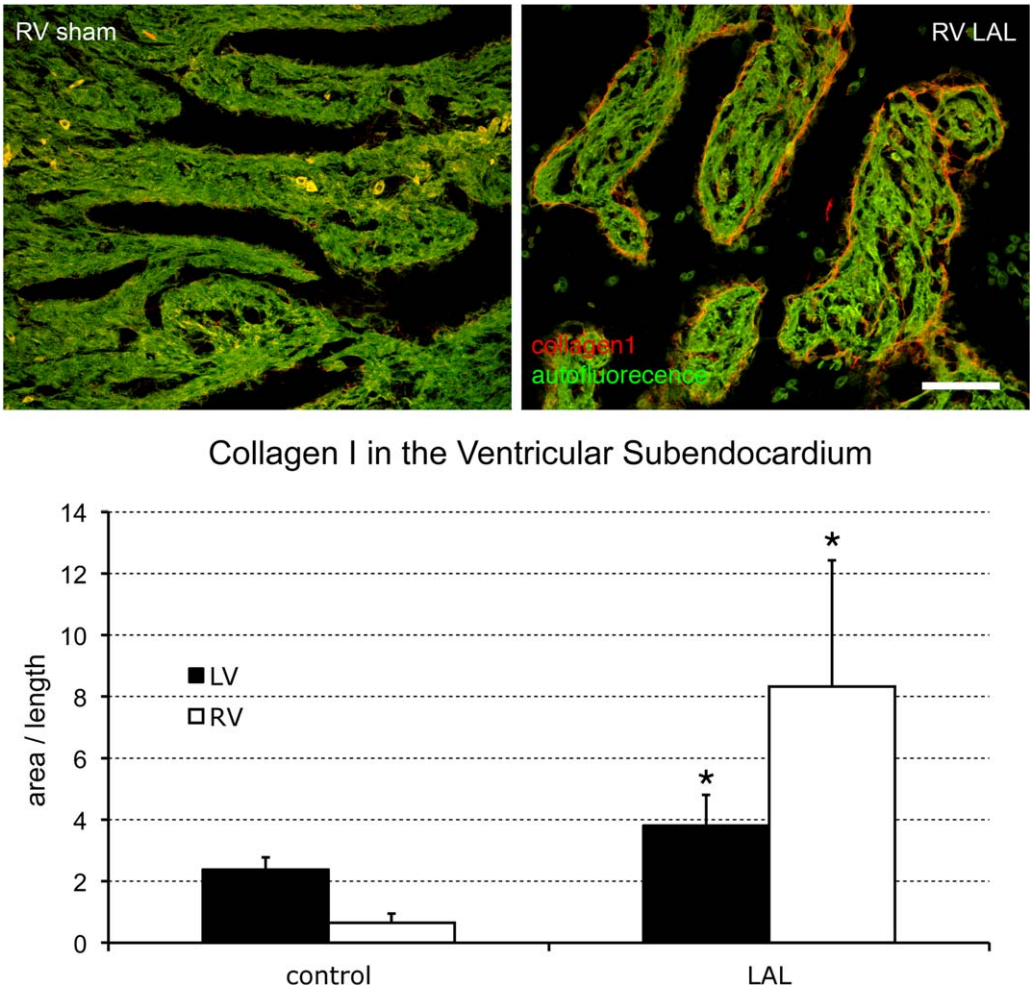

Fig. 2. Increased subendocardial fibrosis in the ED12 LAL hearts. Top panels show examples of images used for quantitative analysis from sham and LAL right ventricle. For left ventricular samples, see Figure 1. Red channel, anti-collagen I; green channel, autofluorescence. Scale bar = 50 μm. Bottom graph demonstrates quantification of the extent of subendocardial collagen-positive layer. The extent of subendocardial immunostaining corrected for endocardial length is significantly increased in both ventricles of the LAL hearts. Data are mean ± SD; n = 6. *$P < 0.05$.

explanation likely, since the hypoxia detected by hypoxyprobe involved the entire left (as well as right) ventricle in the LAL hearts (Fig. 6). Second, the issue of coronary anomalies should be considered; however, those are present only in a subset of LAL hearts, and careful histological analysis showed that in all our LAL samples, both coronary arteries were present, although the left one was, not surprisingly, smaller than usual. Likewise, we detected increased tissue hypoxia at Stage 34/ED8, just prior to normal deployment of coronary arteries, making this explanation unlikely. Third, it was demonstrated that endocardial-to-mesenchymal transformation is not the only source of fibroblasts in the hearts. Other sources, which we can by no means exclude or discount, include epicardially derived cells (Kolditz et al., 2008) or cells from circulation (Zhang et al., 2006). However, since we observed by histology and confocal microscopy mainly increased extracellular matrix in the subendocardium and not increased cellularity (Figs. 4), we suggest that the main source is indeed the endocardium. The second limitation is that we could not demonstrate that there is a molecular response in the endocardium consistent with endocardial-to-mesenchymal transformation in the LAL hearts, despite our efforts to test a panel of antibodies (anti-slug, anti-notch1, anti-ECE1) on this material. In vitro model (e.g., cardiac tissue cultured in a bioreactor allowing more precise manipulation of hemodynamic conditions) (Evans et al., 2003; Tobita et al., 2006) would seem more appropriate for this purpose, as it would in addition allow testing tissues from different periods of development.

The fact that hypoxia influences fibroproduction in the myocardium is supported by literature. The expression of extracellular matrix proteins (fibronectin, collagen I, collagen IV, and laminin) increased over a period of hypoxia in cultured human embryonic stem cells and cardiomyocytes (Horton and Auguste, 2012). Thus, a response to hypoxia by increased collagen production is present even in relatively undifferentiated cells. It has also been shown that angiotensin II-mediated NF-κB signaling via the angiotensin receptor is involved in hypoxia-induced collagen synthesis in human lung fibroblasts (Liu et al., 2013).

Detecting fibrosis in early embryonic tissues is challenging due to their high water content and immaturity of the protein structures. This study demonstrates that periostin immunostaining is a good adjunct to collagen immunodetection in immature tissues (Figs. (1 and 3)). In ED8 and ED12 hearts, standard histological staining with Picrosirius red showed negative results due to the immaturity of the collagen fibers. However, chemical analysis methods detecting collagen by MS (Figs. (5 and 9)) strongly corroborated our histological observations; the relative discrepancy

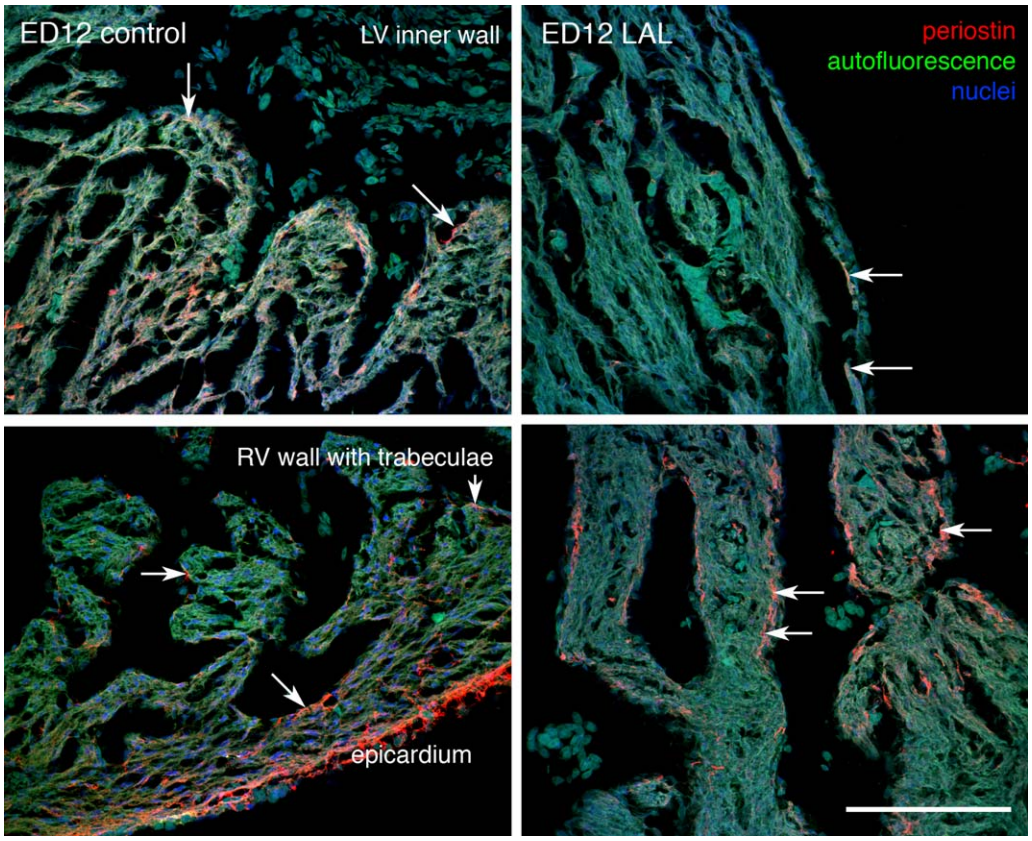

Fig. 3. Anti-periostin staining (red) in ED12 chick embryonic heart. In the left ventricle, the subendocardial staining is patchy and discontinuous in both control and LAL hearts. The sections from the right ventricle (bottom row) show prominent staining in the epicardium and subepicardial mesenchyme; in the control heart, the subepicardial staining is patchy (arrows), like in the left ventricle, and staining is more prominent in the subendocardium overlying the trabeculae in the LAL heart. Scale bar = 100 μm.

in the magnitude of the observed change can be explained by their dilution in MS with tissue homogenization compared to selective quantification of the subendocardial layer by immunohistochemistry (Fig. 2). In this respect, normalization by endocardial length greatly increased the sensitivity of quantification.

Myofibroblasts are a frequent feature in pathological fibrotic tissues (Gourdie et al., 2016), including the EFE in rodent neonatal heart model (Xu et al., 2015), but our anti–smooth muscle staining did not detect their presence in the subendocardium of either normal or LAL hearts. We did, however, observe increased SMA expression in the mesenchyme of both atrioventricular valves (Fig. 4), which are abnormal in this model (Sedmera et al., 1999). It is possible, however, that they may appear in the subendocardium in later progression of the disease or under different etiologies (e.g., inflammatory). Comparison of our data with rodent models also confirms the notion of a critical period for EFE development corresponding roughly to the fetal period. No changes were observed at the end of embryonic period (defined by completion of cardiac septation at ED8 in the chick), and similarly, no fibrosis was induced in 2-week-old (corresponding to childhood) in contrast to neonatal rat hearts (Friehs et al., 2013).

Left ventricular hypoplasia leads to modification of myocardial architecture, altered myocardial differentiation, less contractile protein (Sedmera et al., 1999; Sedmera et al., 2002; de Almeida and Sedmera, 2009), and altered cell properties (Tobita et al., 2005). Some of these changes were observed already with standard histological staining in the original description of the chick model (Sedmera et al., 1999). The significantly increased right ventricular (RV) longitudinal strain and decreased radial and longitudinal strain measured here in LAL hearts may provide insight into possible mechanisms. Acute changes in strain are expected due to the sudden left ventricular (LV) volume underload and RV volume overload. However, the altered strains persisted in the longer term (2 days, from ED4 to ED6), despite the fact that decreased LV loading resulted in 45% smaller tissue volume in LAL hearts, which would otherwise contribute to normalizing LV stress and strain. These results agree with computational models based on measured LV tissue properties in pressure-overloaded conotruncal banding (CTB) and underloaded (verapamil) hearts at comparable developmental stages, showing that neither stress nor strain was normalized in chick from ED4 to ED6, and that changes in material properties are more significant than changes in geometry (Buffinton et al., 2013). The persistent alterations in ventricular strain in LAL hearts underscore the importance of future investigation of mechanical material properties of both ventricles in the HLHS model.

These observed changes in strain are different from strain modifications reported in the HLHS single right ventricle in the human fetus (Brooks et al., 2012), specifically decreased longitudinal relative to circumferential strain, making the RV more similar to the left one. In our study, the circumferential strain of the dilated RV was similar to the normal right (or left) ventricle

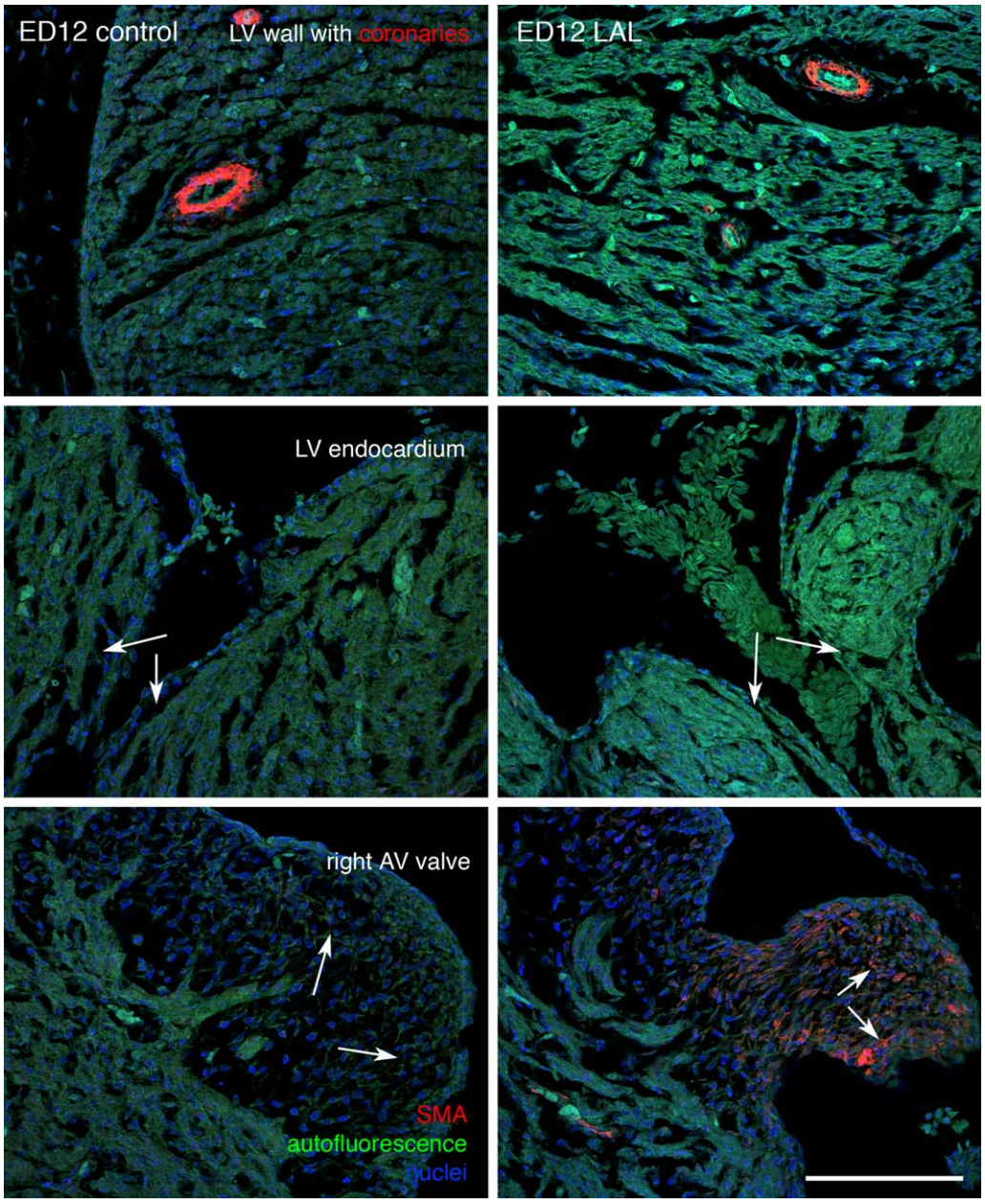

Fig. 4. SMA expression in ED12 control and LAL hearts. Top row shows the LV wall with staining present in the coat of the coronary arteries. Middle row shows lack of staining in the LV subendocardium in both control and LAL hearts. Bottom row shows abundant SMA-positive cells in the mesenchyme of the LAL right atrioventricular valve (septal leaflet), which are not present in the control heart. Scale bar = 100 μm.

(Fig. 7), while the longitudinal strain was significantly increased; we attribute this difference to increased RV size along the longitudinal axis (since it was apex-forming in the LAL hearts), and also to the very early time point in the course of disease progression when the ventricular function was still preserved. It was found that the efficiency of the RV in the human HLHS fetus is reduced, with increased ejection force but decreased cardiac output (Szwast et al., 2009; Brooks et al., 2014), and possibly explaining some neurological deficit in the survivors attributable to the hemodynamic alterations (Limperopoulos et al., 2010), resulting in prenatal brain hypoxia.

As it has been shown that adverse remodeling can be reversed by hemodynamic manipulation at ED8 (deAlmeida et al., 2007), we consider the initial changes observed in this study to be well within the limits of functional plasticity, and the lack of detectable fibrosis before ED12 suggests no stiffening or other irreversible changes at this time point. It is known from postnatal congenital heart disease (e.g., tetralogy of Fallot) that fibrosis in the setting of pulmonary hypertension is to a certain point reversible, so carefully indicated and timed prenatal intervention might prevent development of excessive EFE that might otherwise severely impair LV function and lead to single (right) ventricle circulation with consequent poor prognosis. Whether a prenatal surgical intervention (deAlmeida et al., 2007) or pharmacological approach (Xu et al., 2015) would be more feasible in a clinical setting remains a topic of further investigation.

In conclusion, EFE secondary to altered hemodynamics has been demonstrated in the developing heart. In this case, the heart

is genetically normal. The EFE is associated with and may be caused by tissue hypoxia. Identifying the specific mechanism relating hypoxia to EFE is beyond the scope of this in vivo setup, but could be examined with in vitro experiments.

Experimental Procedures

Left Atrial Ligation (LAL)

White Leghorn chicken embryos were operated on ED4 as previously described (Sedmera et al., 1999). The eggs were reincubated without further turning until ED6, ED8, and ED12 (Hamburger-Hamilton [Hamburger and Hamilton, 1951] Stages 29, 34, and 38, respectively). Sham-operated embryos underwent the windowing and thoracic wall opening. Intact embryos were windowed but unoperated, typically because their position precluded surgical access. Since the sham-operated and intact embryos did not differ in any of the parameters investigated, they were pooled together as the "control" group for statistical purposes. Only hearts with an established phenotype of HLHS, defined as apex-forming right ventricle, were used for further analysis in the LAL group. We analyzed a minimum of six hearts per time point, per group, as detailed below.

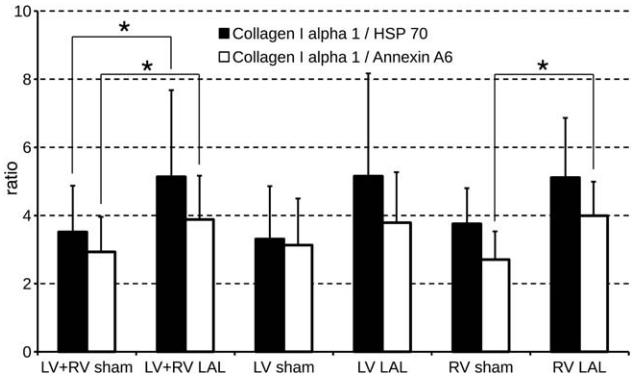

Fig. 5. Quantification of collagen proteins in control and LAL chick embryonic hearts at ED12 using MS. Collagen I normalized by HSP70 or annexin A6 shows an increase in the LAL group. Data from nLC-MS/MS, mean ± SD; n = 8. *$P < 0.05$ (*t*-test).

Echocardiographic and Confocal Examination

Embryos for echocardiographic and confocal study were ligated as described earlier, except the entire procedure was performed in an ex ovo culture setup as described (McQuinn et al., 2007). Echocardiographic examination was performed at ED6 with the Vevo 770 system at 56 fps using two orthogonal imaging planes, resulting in a short-axis and a four-chamber view. From echo loops, the end-systolic and end-diastolic cross-sectional areas of the left ventricle were determined, and global circumferential and radial (in short-axis view, midportion) and longitudinal (in four-chamber view) strains were measured on still frames. The measurements were performed for the whole epicardial circumference to avoid ambiguities in landmarks shifting out of plane of focus. For comparison, the absolute value of the difference (diastolic minus systolic state) was used, resulting in all the active strains having positive values.

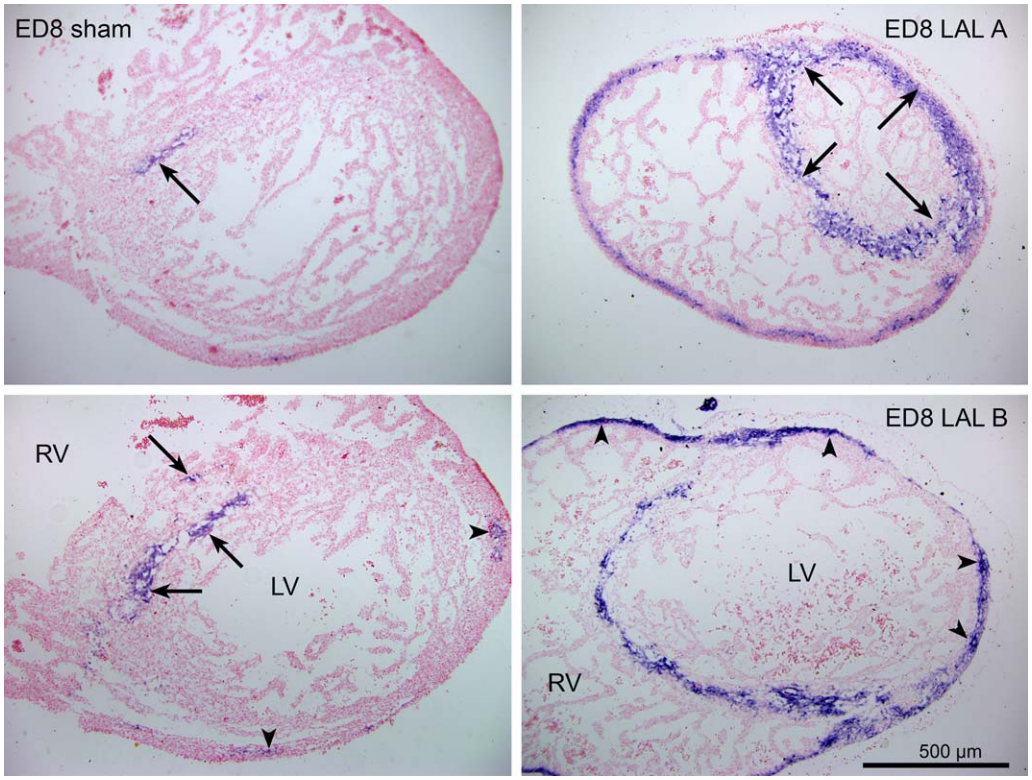

Fig. 6. Hypoxic regions in ED8 chick embryonic heart. Short-axis views showing restricted hypoxyprobe staining the control heart, limited to the interventricular septum (arrows) and patches in the left ventricular compact zone (arrowheads), contrasting with widespread hypoxia in the compact myocardium of the LAL hearts (two different examples shown). LV, left ventricle; RV, right ventricle.

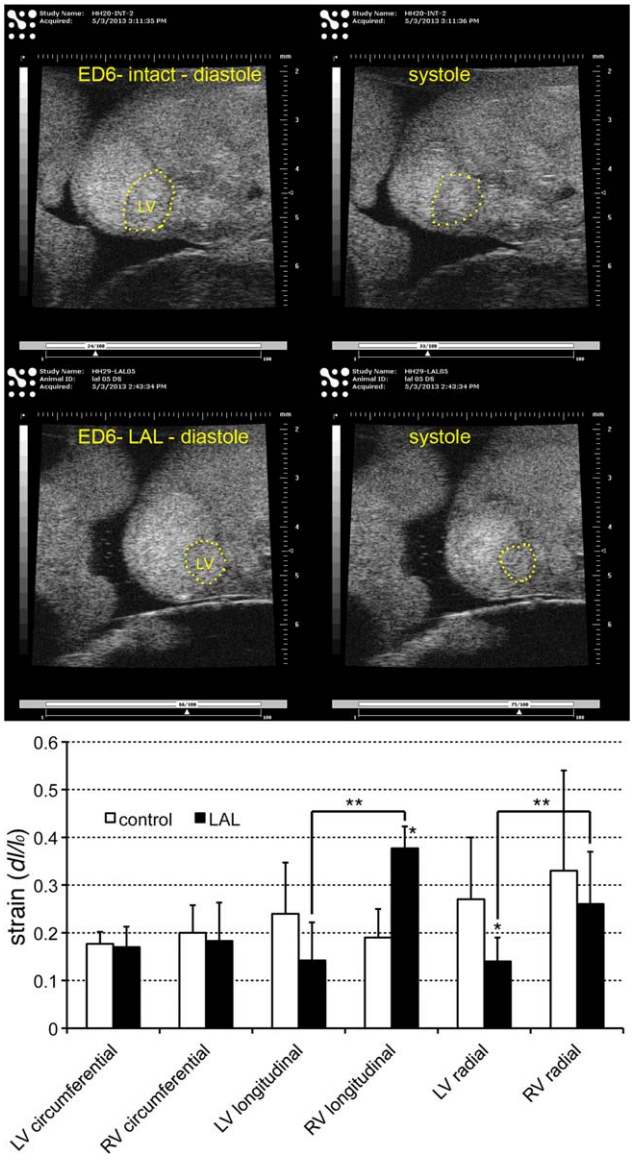

Fig. 7. Ultrasound biomicroscopy of chick embryonic hearts at ED6. Left ventricle (outlined by dots) is significantly smaller in the LAL hearts with developed phenotype (apex-forming right ventricle), but its function (ejection fraction) remains normal at this stage. Strain analysis (bottom) shows near-normal circumferential but mildly reduced longitudinal and significantly decreased radial strain in the smaller left ventricle together with increased longitudinal strain in the volume-overloaded right ventricles. Data (absolute values) are mean ± SD; n = 6. $^{*}P < 0.05$ vs. control, $^{**}P < 0.05$ RV vs. LV.

After examination, the embryos were dissected free from the membranes, perfusion-fixed with 4% paraformaldehyde in phosphate buffer saline (PBS), and, after ethanol dehydration and benzyl alcohol:benzyl benzoate (BABB) clearing, imaged whole-mount on an Olympus FluoView confocal microscope using a 10x, 0.4 NA objective at 2.5-micron z-step and z-brightness compensation as described (Miller et al., 2005). Stacks of TIFF images from confocal microscopy were loaded into Amira v6.0 software (FEI, Hillsboro, OR) with pixel sizes set at 3.2125 µm in *x* and *y* and 3.125 µm in *z*, assuming 80% isotropic shrinkage from benzyl alcohol:benzyl benzoate as reported in Kolesová et al. (2016). When more than one stack was used to cover the *xy* plane, an affine registration module performed automatic alignment to stich the stacks, followed by stack transformation and merging. Alignment was verified by inspection. The images were filtered with a contrast-limited adaptive histogram equalization (CLAHE) routine with contrast limit of 7. For volume calculation, automatic thresholding by gray scale value separated tissue from background, followed by island removal and label smoothing (Gaussian filtering). Further segmentation of the left ventricle was done by manual tracing with pen tablet on each image to separate the left ventricle and the entire septum from the right ventricle, developing valves, and atria, as well as the volume of the segmented left ventricle and septum measured.

Histological Examination

Sampling was performed at ED8 and ED12. The hearts were fixed in 4% paraformaldehyde and processed into paraffin. Alternating routine paraffin sections of 10-µm thickness were stained with Alcian blue/hematoxylin-eosin or antibodies directed against periostin (1:100; Abcam, ab14041) or collagen I (1:500; MD Biosciences, 203002) and detected with donkey anti-rabbit secondary antibody coupled with Rhodamine red (Jackson ImmunoResearch Laboratories, Inc.). The slides for collagen staining were heat-treated twice for 5 min in citrate buffer (pH 6.0) before blocking for antigen retrieval. The nuclei were counterstained with Hoechst 33342 (Sigma). Additional staining was performed with anti-SMA antibody (clone 1A4, Sigma, 1:1000) to detect the possible presence of myofibroblasts in the subendocardium.

The stained sections were mounted into DEPEX (Electron Microscopy Sciences) and examined with an Olympus FluoView confocal laser-scanning microscope using 10x (overview picture) dry and 40x oil immersion objectives. The area of anti-collagen immunostaining was quantified on five successive confocal sections obtained with a 1-µm z-step at 40x magnification and normalized against the length of the endocardial surface in the field of view using ImageJ (National Institutes of Health).

Staining for hypoxic regions was performed after intravenous injection of pimonidazole hydrochloride at ED8 in six control and six LAL hearts as described (Nanka et al., 2008) using anti-pimonidazole mouse IgG1 monoclonal antibody (1:50; Hypoxyprobe, MAb1 Lot # 9.7.11). These sections were examined using transmitted light on an Olympus BX50 upright microscope and documented by an Olympus DP 71 CCD camera.

Protein Detection via MS

Sample preparation

The samples (eight control and eight LAL hearts with confirmed phenotype at ED12) were microdissected into the left ventricle (including the septum) and right ventricle. Microdissection of hearts as young as ED6 was successfully used previously to measure quantitatively expression of various genes and proteins (Krejci et al., 2012). It was essential in this case, as other cardiac compartments (e.g., valves and great arteries) contain significantly more connective tissue than the ventricles, so careful separation of different compartments allowed meaningful comparison of collagen protein amounts in the ventricles without contamination from other sources. All samples were washed three times in physiological solution, once in 0.2 mL of a solution containing NH_4HCO_3 (0.05 mol/L) and heated at 105 °C for 5 min. Samples were then digested in a solution containing NH_4HCO_3 (0.05 mol/L) and trypsin (0.2 mg/mL; Sigma, St. Louis, MO,) 1/50

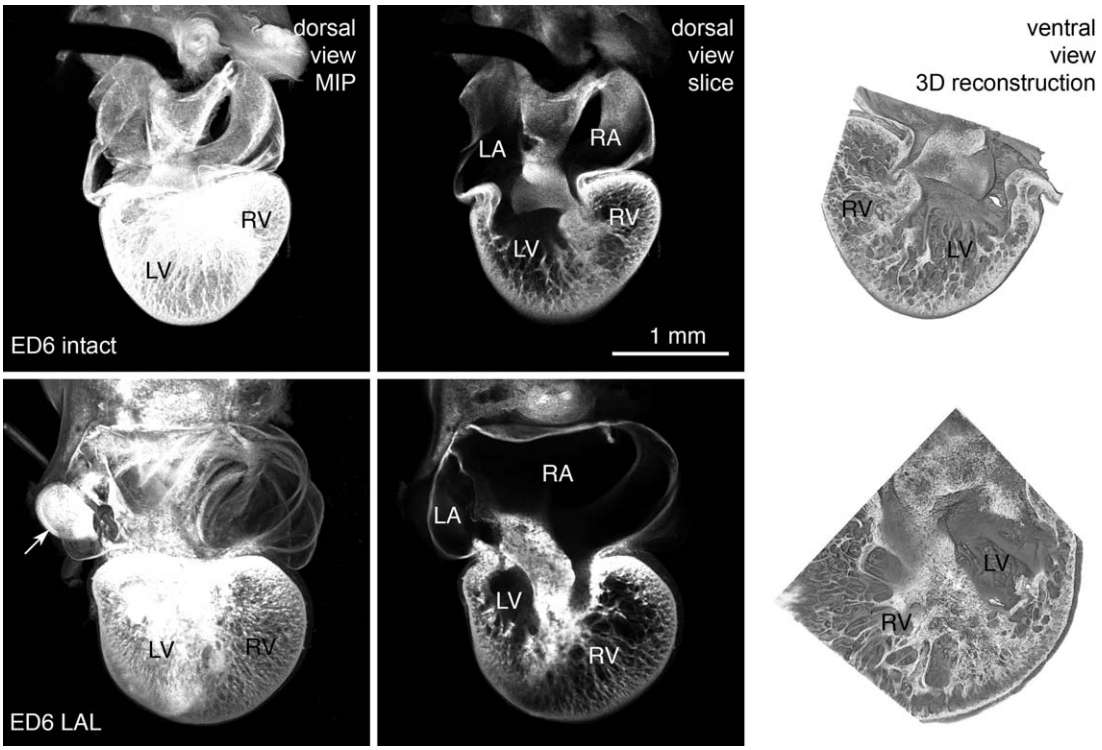

Fig. 8. Left ventricular myocardial architecture at ED6. Dorsal views of maximum-intensity confocal projections and single sections of ED6 hearts taken using 4x objective. Three-dimensional reconstruction of confocal microscopy series taken with 10x lens shows that the LAL hearts have smaller left ventricle. LA, left atrium; LV, left ventricle; RA, right atrium; RV, right ventricle.

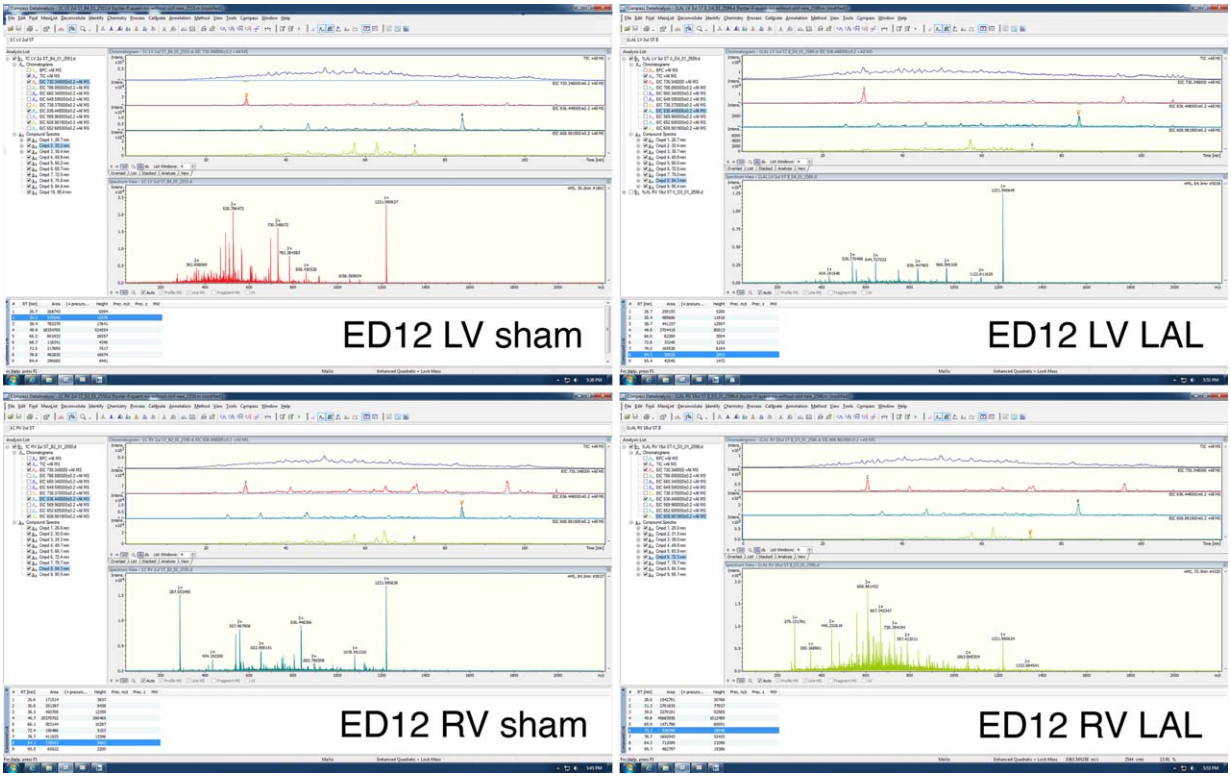

Fig. 9. Examples of MS spectra of sample from the control and LAL hearts. Chromatograms are described from the top: 1) total ion chromatogram (TIC); 2) MS spectrum of specific peptide of collagen I α1; 3) MS spectrum of specific peptide of annexin A6; 4) MS spectrum of specific peptide of HSP70. The spectrum in the middle part of each picture is MS/MS spectrum of specific peptide of collagen I α1. The bottom table panel shows the integration of peaks, which corresponds to the concentration of specific peptides of proteins.

TABLE 1. Raw Data of MS Measurements (Specific Peptides of HSP70 and Collagen I)

	HSP70 (608,982 M/Z)	HSP70 (608,982 M/Z)	Collagen I (786.891 M/Z)	Collagen I (786.891 M/Z)
Samples	Control HSP70	LAL HSP70	Control Collagen I	LAL Collagen I
1. LV	217695	33240	783279	441157
1. RV	150486	528390	450708	3279191
2. LV	132661	264518	278727	914941
2. RV	92637	188584	233489	629541
3. LV	199372	206652	1303914	673344
3. RV	X	181121	476057	1439753
4. LV	138659	141765	220531	771934
4. RV	84399	X	295333	47560
5. LV	237933	115445	530634	329996
5. RV	156271	129916	558465	523716
6. LV	247960	222603	739805	722177
6. RV	196531	93581	812148	567183
7. LV	242131	74811	994632	406372
7. RV	221922	169292	1288635	959814
8. LV		316351		1399044
8. RV		167760		421922
9. LV		122368		609073

TABLE 2. Raw Data of MS Measurements (Specific Peptides of Annexin A6 and Collagen I)

	Annexin A6 (836.448 M/Z)	Annexin A6 (836.448 M/Z)	Collagen I (786.891 M/Z)	Collagen I (786.891 M/Z)
Samples	Control annexin A6	LAL annexin A6	Control collagen I	LAL collagen I
1. LV	290685	58928	783279	441157
1. RV	278503	712089	450708	3279191
2. LV	150901	336508	278727	914941
2. RV	143550	198863	233489	629541
3. LV	268128	223014	1303914	673344
3. RV	158699	299513	476057	1439753
4. LV	157428	249183	220531	771934
4. RV	85742	23420	295333	47560
5. LV	155479	166917	530634	329996
5. RV	201779	112560	558465	523716
6. LV	179875	169844	739805	722177
6. RV	215118	111023	812148	567183
7. LV	280025	100801	994632	406372
7. RV		220489	1288635	959814
8. LV		333300		1399044
8. RV		132090		421922
9. LV		185149		609073

(w/w - trypsin/sample) for 16 hr at 37 °C. Samples were once again treated at 105 °C for 5 min, lyophilized, and digested in solution containing NH_4HCO_3 (0.05 mol/L) and trypsin (0.2 mg/mL) (1/50 w/w-trypsin/sample) at 37 °C overnight. Stage Tips (Rappsilber et al., 2007) aided purification of samples for nLC-MS/MS. Extracted solutions were lyophilized and dissolved in 100 µL of 1% formic acid.

Analysis of tryptic digests with LC-MS/MS

The separation of peptides was achieved via a linear gradient between mobile phases A (water) and B (acetonitrile), both containing 0.1% (v/v) formic acid. The separation and online nanoelectrospray ionization was performed as described (Ost'adal et al., 2015).

The nano-LC apparatus used for analysis of the protein digests was a Proxeon Easy-nLC (Proxeon, Odense, Denmark) coupled to a maXis Q-TOF (quadrupole–time of flight) mass spectrometer with ultra-high resolution (Bruker Daltonics, Bremen, Germany) by nanoelectrosprayer. The nLC-MS/MS instruments were controlled with the software packages HyStar 3.2 and micrOTOF-control 3.0. The data were collected and analyzed using the software packages ProteinScape 3.0 and Data Analysis 4.0 (Bruker

Daltonics). Peptide mixtures were injected into a NS-AC-11-C18 Biosphere C18 column (particle size: 5 μm; pore size: 12 nm; length: 150 mm; inner diameter: 75 μm) with a NS-MP-10 Biosphere C18 pre-column (particle size: 5 μm; pore size: 12 nm; length: 20 mm; inner diameter: 100 μm), both obtained from NanoSeparations (Nieuwkoop, Netherlands). All nLC-MS and LC-MS/MS analyses were performed in duplicate.

Peptides specific for collagen I, HSP70, and annexin A6, obtained by trypsin digestion, were selected for assessment. Each of these marker peptides had to meet all of the following criteria simultaneously: 1) they had to be detected in all samples; 2) their peak area in nLC-MS/MS chromatograms of the samples had to be reproducible; and 3) they had to be unique to the individual protein (i.e., the peptide could not be part of any other protein structure in the SwissProt/NCBI databases). Use of normalization standards for quantification of the MS peaks in spectra is necessary, and the choice of annexin A6 and HSP70 as housekeeping standards is supported by recent literature (Murphy, 2013). We used therefore two proteins, HSP70 and annexin A6, as comparative proteins for collagen I. The HSP70 was selected for its housekeeping functions as transport of proteins between cellular compartments, degradation of unstable and misfolded proteins, prevention and dissolution of protein complexes, folding and refolding of proteins, uncoating of clathrin-coated vesicles, and control of regulatory proteins (chaperone protein). The annexin A6 (lipid-binding protein) was used as the second control protein. The peptides corresponding to both these proteins were abundantly present in control and LAL groups.

Changes in the relative protein quantity were determined according to the peak area of selected specific peptides in the MS spectra. The selected peptide spectra for the individual proteins were: collagen I α1 (sequence: K.GATGAPGIAGAPGFPGAR.G, m/z 786.8906, z = 2); HSPA9 Stress-70 protein (R.VEAVNLAEGIIHDTESK.M, m/z 608.9812, z = 3); annexin A6 (K.GLGTDEGAIIEVLTQR.S, m/z 836.4482, z=2). Peak detection from the MS spectra and their integration is shown in Figure 9. Raw data illustrating the peaks together with individual values from samples are included in Tables 1 and 2.

Database search

Database searches were performed as described (Jagr et al., 2012), with the taxonomy restricted to *Gallus gallus* to remove protein identification redundancy. Only significant hits (MASCOT score-≥ 80, http://www.matrixscience.com) were accepted.

Acknowledgments

We are grateful to Ms. Jarmila Svatunkova, Marie Jindrakova, and Klara Krausova for their excellent technical assistance, and to Mr. Vojtech Cerny for help with the left atrial ligations.

References

Achiron R, Malinger G, Zaidel L, Zakut H. 1988. Prenatal sonographic diagnosis of endocardial fibroelastosis secondary to aortic stenosis. Prenat Diagn 8:73–77.

Angelov A, Kulova A, Gurdevsky M. 1984. Endocardial fibroelastosis. Clinico-pathological study of 38 cases. Pathol Res Pract 178:384–388.

Bohlmeyer TJ, Helmke S, Ge S, Lynch J, Brodsky G, Sederberg JH, Robertson AD, Minobe W, Bristow MR, Perryman MB. 2003. Hypoplastic left heart syndrome myocytes are differentiated but possess a unique phenotype. Cardiovasc Pathol 12:23–31.

Bradley SM. 1999. Neonatal repair and dealing with a single ventricle. J S C Med Assoc 95:335–338.

Brooks PA, Khoo NS, Hornberger LK. 2014. Systolic and diastolic function of the fetal single left ventricle. J Am Soc Echocardiogr 27:972–977.

Brooks PA, Khoo NS, Mackie AS, Hornberger LK. 2012. Right ventricular function in fetal hypoplastic left heart syndrome. J Am Soc Echocardiogr 25:1068–1074.

Buffinton CM, Faas D, Sedmera D. 2013. Stress and strain adaptation in load-dependent remodeling of the embryonic left ventricle. Biomech Model Mechanobiol 12:1037–1051.

Dbaly J, Rychter Z. 1967. The vascular system of the chick embryo. XVII. The development of branching of the coronary arteries in the chick embryos with experimentally induced left-half heart hypoplasy. Folia Morphol (Praha) 15:358–368.

deAlmeida A, Sedmera D. 2009. Fibroblast Growth Factor-2 regulates proliferation of cardiac myocytes in normal and hypoplastic left ventricles in the developing chick. Cardiol Young 19:159–169.

deAlmeida A, McQuinn T, Sedmera D. 2007. Increased ventricular preload is compensated by myocyte proliferation in normal and hypoplastic fetal chick left ventricle. Circ Res 100:1363–1370.

Essed CE, Klein HW, Krediet P, Vorst EJ. 1975. Coronary and endocardial fibroelastosis of the ventricles in the hypoplastic left and right heart syndromes. Virchows Arch A Pathol Anat Histol 368:87–97.

Evans HJ, Sweet JK, Price RL, Yost M, Goodwin RL. 2003. Novel 3D culture system for study of cardiac myocyte development. Am J Physiol Heart Circ Physiol 285:H570–578.

Fishman NH, Hof RB, Rudolph AM, Heymann MA. 1978. Models of congenital heart disease in fetal lambs. Circulation 58:354–364.

Friehs I, Illigens B, Melnychenko I, Zhong-Hu T, Zeisberg E, Del Nido PJ. 2013. An animal model of endocardial fibroelastosis. J Surg Res 182:94–100.

Gourdie RG, Dimmeler S, Kohl P. 2016. Novel therapeutic strategies targeting fibroblasts and fibrosis in heart disease. Nat Rev Drug Discov 15:620–638.

Grossfeld PD. 1999. The genetics of hypoplastic left heart syndrome. Cardiol Young 9:627–632.

Hamburger V, Hamilton HL. 1951. A series of normal stages in the development of the chick embryo. J Morphol 88:49–92.

Harh JY, Paul MH, Gallen WJ, Friedberg DZ, Kaplan S. 1973. Experimental production of hypoplastic left heart syndrome in the chick embryo. Am J Cardiol 31:51–56.

Horton RE, Auguste DT. 2012. Synergistic effects of hypoxia and extracellular matrix cues in cardiomyogenesis. Biomaterials 33:6313–6319.

Jagr M, Eckhardt A, Pataridis S, Miksik I. 2012. Comprehensive proteomic analysis of human dentin. Eur J Oral Sci 120:259–268.

Kolditz DP, Wijffels MC, Blom NA, van der Laarse A, Hahurij ND, Lie-Venema H, Markwald RR, Poelmann RE, Schalij MJ, Gittenberger-de Groot AC. 2008. Epicardium-derived cells in development of annulus fibrosis and persistence of accessory pathways. Circulation 117:1508–1517.

Kolesova H, Capek M, Radochova B, Janacek J, Sedmera D. 2016. Comparison of different tissue clearing methods and 3D imaging techniques for visualization of GFP-expressing mouse embryos and embryonic hearts. Histochem Cell Biol 146:141–152.

Krejci E, Pesevski Z, DeAlmeida AC, Mrug M, Fresco VM, Argraves WS, Barth JL, Cui X, Sedmera D. 2012. Microarray analysis of normal and abnormal chick ventricular myocardial development. Physiol Res 61 Suppl 1:S137–144.

Limperopoulos C, Tworetzky W, McElhinney DB, Newburger JW, Brown DW, Robertson RL Jr, Guizard N, McGrath E, Geva J, Annese D, Dunbar-Masterson C, Trainor B, Laussen PC, du Plessis AJ. 2010. Brain volume and metabolism in fetuses with congenital heart disease: evaluation with quantitative magnetic resonance imaging and spectroscopy. Circulation 121:26–33.

Liu SS, Wang HY, Tang JM, Zhou XM. 2013. Hypoxia–induced collagen synthesis of human lung fibroblasts by activating the angiotensin system. Int J Mol Sci 14:24029–24045.

Loffredo CA, Chokkalingam A, Sill AM, Boughman JA, Clark EB, Scheel J, Brenner JI. 2004. Prevalence of congenital

cardiovascular malformations among relatives of infants with hypoplastic left heart, coarctation of the aorta, and d-transposition of the great arteries. Am J Med Genet A 124:225–230.
McQuinn TC, Bratoeva M, Dealmeida A, Remond M, Thompson RP, Sedmera D. 2007. High-frequency ultrasonographic imaging of avian cardiovascular development. Dev Dyn 236:3503–3513.
Miller CE, Thompson RP, Bigelow MR, Gittinger G, Trusk TC, Sedmera D. 2005. Confocal imaging of the embryonic heart: How deep? Microscop Microanal 11:216–223.
Murphy ME. 2013. The HSP70 family and cancer. Carcinogenesis 34:1181–1188.
Nanka O, Krizova P, Fikrle M, Tuma M, Blaha M, Grim M, Sedmera D. 2008. Abnormal myocardial and coronary vasculature development in experimental hypoxia. Anat Rec (Hoboken) 291:1187–1199.
Nield LE, Silverman ED, Taylor GP, Smallhorn JF, Mullen JB, Silverman NH, Finley JP, Law YM, Human DG, Seaward PG, Hamilton RM, Hornberger LK. 2002. Maternal anti-Ro and anti-La antibody-associated endocardial fibroelastosis. Circulation 105:843–848.
Ost'adal M, Eckhardt A, Herget J, Miksik I, Dungl P, Chomiak J, Frydrychova M, Burian M. 2015. Proteomic analysis of the extracellular matrix in idiopathic pes equinovarus. Mol Cell Biochem 401:133–139.
Rappsilber J, Mann M, Ishihama Y. 2007. Protocol for micro-purification, enrichment, pre-fractionation and storage of peptides for proteomics using StageTips. Nat Protoc 2:1896–1906.
Rychter Z, Rychterova V. 1981. Angio- and Myoarchitecture of the Heart Wall under Normal and Experimentally changed Morphogenesis. In: Pexieder T, editor. Perspectives in Cardiovascular Research. New York: Raven Press. p 431–452.
Sedmera D, Cook AC, Shirali G, McQuinn TC. 2005. Current issues and perspectives in hypoplasia of the left heart. Cardiol Young 15:56–72.
Sedmera D, Hu N, Weiss KM, Keller BB, Denslow S, Thompson RP. 2002. Cellular changes in experimental left heart hypoplasia. Anat Rec 267:137–145.
Sedmera D, Pexieder T, Rychterova V, Hu N, Clark EB. 1999. Remodeling of chick embryonic ventricular myoarchitecture under experimentally changed loading conditions. Anat Rec 254:238–252.
Szwast A, Tian Z, McCann M, Donaghue D, Rychik J. 2009. Right ventricular performance in the fetus with hypoplastic left heart syndrome. Ann Thorac Surg 87:1214–1219.
Tobita K, Garrison JB, Li JJ, Tinney JP, Keller BB. 2005. Three-dimensional myofiber architecture of the embryonic left ventricle during normal development and altered mechanical loads. Anat Rec A Discov Mol Cell Evol Biol 283:193–201.
Tobita K, Liu LJ, Janczewski AM, Tinney JP, Nonemaker JM, Augustine S, Stolz DB, Shroff SG, Keller BB. 2006. Engineered early embryonic cardiac tissue retains proliferative and contractile properties of developing embryonic myocardium. Am J Physiol Heart Circ Physiol 291:H1829–1837.
Weinberg T, Himmelfarb AJ. 1943. Endocardial fibroelastosis. Bull Johns Hopkins Hosp 72:299.
Wikenheiser J, Doughman YQ, Fisher SA, Watanabe M. 2006. Differential levels of tissue hypoxia in the developing chicken heart. Dev Dyn 235:115–123.
Xu X, Friehs I, Zhong Hu T, Melnychenko I, Tampe B, Alnour F, Iascone M, Kalluri R, Zeisberg M, Del Nido PJ, Zeisberg EM. 2015. Endocardial fibroelastosis is caused by aberrant endothelial to mesenchymal transition. Circ Res 116:857–866.
Zhang N, Mustin D, Reardon W, Almeida AD, Mozdziak P, Mrug M, Eisenberg LM, Sedmera D. 2006. Blood-borne stem cells differentiate into vascular and cardiac lineages during normal development. Stem Cells Dev 15:17–28.
Zhang Z, Nie F, Kang C, Chen B, Qin Z, Ma J, Ma Y, Zhao X. 2014. Increased periostin expression affects the proliferation, collagen synthesis, migration and invasion of keloid fibroblasts under hypoxic conditions. Int J Mol Med 34:253–261.